Detection and Analysis of an Eave Purlin of the Timber Building Eroded by Carpenter Bees Based on Computed Tomography

Xiaoxia Yang,[a] Yisheng Gao,[b,*] Ziyu Zhao,[a] Zhedong Ge,[a] Xiaoping Liu,[a] and Yucheng Zhou [a]

To explore the harm of carpenter bee nests to timber buildings, an eave purlin of Wu's house, the seventh batch of national key cultural relics in China, was taken as the research object. A CT (computed tomography) device was used to collect the projection data of wood components, and VGSTUDIO MAX3.2 software was used to reconstruct multiple transverse sections, radial sections, tangential sections, and 3D (three-dimensional) images of an eave purlin. The results showed that carpenter bees eroded on a timber building randomly, but they usually nested along the length of eave purlin. The wood in the middle of an eave purlin is more vulnerable to carpenter bees than the end. Carpenter bee nests are usually not connected, and the volume of nests accounts for 3% to 4% of the eave purlin. The eave purlin is applied with an orientation and a torsion force. The position of the maximum hot spots of the stress occurs at holes and the large cracks, indicating that carpenter bee nests have a great impact on the mechanical properties of timber buildings. The research results of this paper provide reference for the safety evaluation and preventive protection of timber buildings.

DOI: 10.15376/biores.17.2.2443-2456

Keywords: Timber building; Carpenter bee; Non-destructive testing; CT; Mechanical property analysis

*Contact information: a: School of Information and Electrical Engineering, Shandong Jianzhu University, Jinan, Shandong 250101, China; b: School of Architecture and Urban Planning, Shandong Jianzhu University, Jinan, Shandong 250101, China; *Corresponding author: gao_sdjz@126.com*

INTRODUCTION

Timber buildings have formed a unique style and structural system after thousands of years of development and are also an important part of Chinese culture with a rich historical research value (Annila *et al.* 2018; Zhang *et al.* 2021). At present, timber buildings in southern China are mostly eroded by carpenter bees and termites. It is difficult to obtain the internal information of components from the building surface and the impact of damage on the mechanical properties of buildings (Eriksen *et al.* 2016; Charles *et al.* 2018; Bukauskas *et al.* 2019; Ma *et al.* 2019). Therefore, it is meaningful to study the distribution law and stress hot spot positions of carpenter bee nests in building components, which is important for the safety and preventive protection of timber buildings.

Time and external environment lead to the destruction of timber building components. For example, the change of temperature and humidity leads to the cracking of wood components, which will also aggravate the erosion of insects or fungi, resulting in holes or decay in timber building components (Rashidi *et al.* 2020). At present, ultrasonic and stress waves are mainly used as timber building detection methods (Du *et al.* 2018;

Vössing and Niederleithinger 2018; Llana *et al.* 2020), and some researchers have applied the above technology to the detection and evaluation of building safety (Sousa *et al.* 2013; Jiao *et al.* 2019). Although nondestructive testing can be used to evaluate the safety and reliability of timber buildings, the image results obtained by the above methods are not accurate. By contrast, CT could reconstruct clear images inside the object, which should be used for the nondestructive testing of timber buildings. There are many researchers who have applied CT to wood research, but there are few papers on the detection and mechanical property simulation analysis of timber building components eroded by insects. Computed tomography was used to reconstruct 2D (two-dimensional) and 3D images of wood. These images can show the position, shape, volume, density, and moisture content of the internal structures of wood, such as the pith, the sapwood, the heartwood, and the knots (Wei *et al.* 2011; Pan *et al.* 2021). Ge *et al.* (2018) developed a set of CT systems to detect immovable objects, such as building support components and living trees, and reconstructed high-quality images to analyze the characteristics of wood structure and visualize the internal structure of immovable objects. Although some components of buildings are large and fixed and immovable, CT can be used to evaluate and analyze structures having internal damage.

It can be seen from the referenced literature that it is feasible to detect timber building components by nondestructive testing, but nests and stress hot spots distribution of timber building components eroded by carpenter bees have not been studied by researchers. An eave purlin, removed from the famous Wu's mansion in Ningde City, Fujian province, China, is taken as the research object in this paper because the component can represent a kind of timber building eroded by carpenter bees. The detection and protection of these timber buildings is important and urgent. The purpose of this study is to provide reference for the subsequent detection and preventive protection of timber buildings.

EXPERIMENTAL

Experimental Materials and Equipment

Fengqi Wu's mansion in Zherong County, Ningde City, Fujian Province (27.19 °N, 120.06 °E) is a timber building (You 2016). Eave purlins are important building components that bear the weight of the roof. It is necessary to study the influence of carpenter bees on it. Figures 1 (a) and (b) show a photo of the eave purlin, where the part selected with the red box is the eave purlin. Obvious holes left by carpenter bees can be seen from the surface of the eave purlin. It can be seen from part (b) of the figure that the eaves purlin seriously damaged by carpenter bees has been replaced, and the part selected with the blue box is the replaced eave purlin. In the timber buildings, one of the eave purlins was built with *Cunninghamia*, 3000 mm in length and 250 mm in diameter. Because the eave purlin was too long for shipment, it was cut into three logs (Log A: 977.7 mm long, Log B: 998.5 mm long, and Log C: 990.1 mm long). There were some holes on the surface of the eave purlin, which were caused by carpenter bees. To estimate the degree of wood damage after being eroded by carpenter bees, logs were scanned on a CT (SIEMENS SOMATOM Definition AS, Berlin, Germany). The CT collected the attenuation data of X-ray energy after passing through the log, and the images of defects and holes in the log were reconstructed. The voltage and current of the X-ray source were set to 120 kV and

300 mAs, respectively, slice thickness of 0.5 mm, and a slice increment of 0.5 mm in Shandong Jianzhu University in Jinan, China.

Fig. 1. Photos of eave purlin in ancient wooden structures; (a) The Eave purlin before replacement; (b) A purlin component has been replaced

2D Images Reconstruction

The 2D images of wood were obtained after CT scanning, as shown in Fig. 2. Multiple planes passing through the pith of the log were made as virtual planes separating the log. The number of virtual planes was expressed as n and the angle was expressed as θ. Their relationship can be expressed as $n = \pi / \theta$. The images generated by these virtual planes were the radial sections of logs, as shown in Figs. 2 (c) and (f). Many radial sections can be obtained by this method, which cannot be realized by traditional methods.

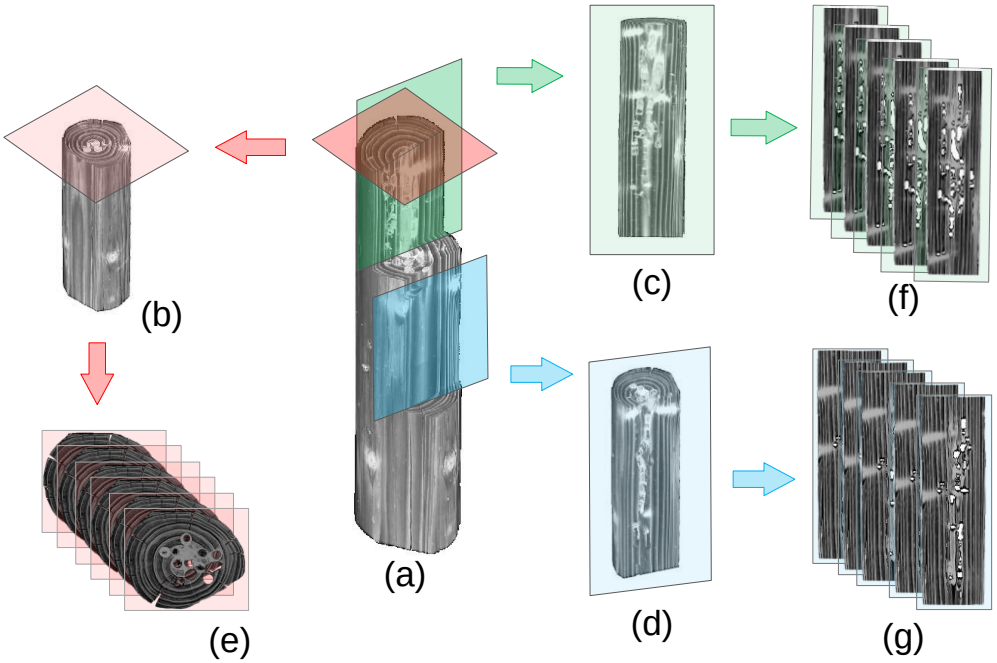

Fig. 2. 3D and 2D images of three sections of logs: (a) log specimen; (b) the transverse section in 3D; (c) the radial section in 3D; (d) the tangential section in 3D; (e) the transverse sections in 2D; (f) the radial sections in 2D; (g) the tangential sections in 2D

Based on CT technology, the transverse sections of the log referred to the section perpendicular to the growth direction of the trunk main axis, as shown in Figs. 2 (b) and (e). Tangential sections referred to the longitudinal section of the trunk that did not pass through the pith core, as shown in Figs. 2. (d) and (g). Figure 2 (a) shows the 3D structure of the log. From this picture, the transverse, radial, and tangential sections can be seen. As shown in Fig. 2., the log was cut with the red, green, and blue planes, so multiple 2D images of wood transverse, radial, and tangential sections could be obtained.

3D Images Reconstruction

The CT data files in DICOM format of Log A, Log B, and Log C were loaded using VG Studio MAX software (Volume Graphics GmbH, VG Studio MAX3.2, Heidelberg, Germany) to generate images with a size of 512 × 512. Because the holes reduce the bearing capacity of the eave purlin, the features of interest in images were selected, and the region growth method was used to extract the holes in transverse sections. Multiple transverse sections were arranged in scanning order, and a 3D image was generated. In the 3D image, a surface fitting with the surface of log was constructed, and the elastic modulus and Poisson's ratio of Cunninghamia lanceolata were set to 1.0×10^{10} Pa and 0.33. One end of the log was fixed and a force was applied at the other end to analyze the hot spots distribution of the log under directional force and torsion force.

RESULTS AND DISCUSSION

Statistics of the Number of Holes

To obtain the distribution information of carpenter bee nests, multiple sections of logs were reconstructed, and each section was perpendicular to the growth direction of logs. As shown in Fig. 3., X coordinate represents the section number of each log, and Y coordinate represents the number of cross-sectional holes in the carpenter bee nests. Log A was damaged by carpenter bees from the 591st layer, and the damage gradually increased from the first hole, which was 295.5 mm away from the end of Log A. The 1411st to 1469th layers of logs were the most seriously eroded by carpenter bees, corresponding to 705.50 mm to 734.5 mm of Log A. There were at most 16 holes in a layer. Log B was the middle part of the eave purlin. There were only three holes in the first layer. The most seriously eroded by carpenter bees were the 1060th to 115th layers, which are located at 530 mm to 579.5 mm of Log B. There are at most 13 holes in a layer. The most serious damage of Log C by carpenter bees is from the 1062nd to 1085th layers, which were located at 531 mm to 542.5 mm. There were at most 15 holes in a layer. After the 1319th layer of Log C, the structure between 659.5 mm to 990.1 mm was not damaged by carpenter bees, because this part was the end of the eave purlin. Consistent with the previous inference, the end of the eave purlin is not easy to be eroded by carpenter bees, and the middle structure was most seriously damaged.

According to the distribution of carpenter bee nests in the eave purlin, both ends of the eave purlin were not eroded by carpenter bees. The direction of wood erosion by carpenter bees is random, so an eave is usually eroded by carpenter bees, resulting in multiple unconnected nests. Carpenter bees like to live in a high temperature environment, and the components near the flowers are vulnerable to carpenter bees (Pando *et al*. 2011; Azmi *et al*. 2012), so preventive protection measures must be taken in advance in this area.

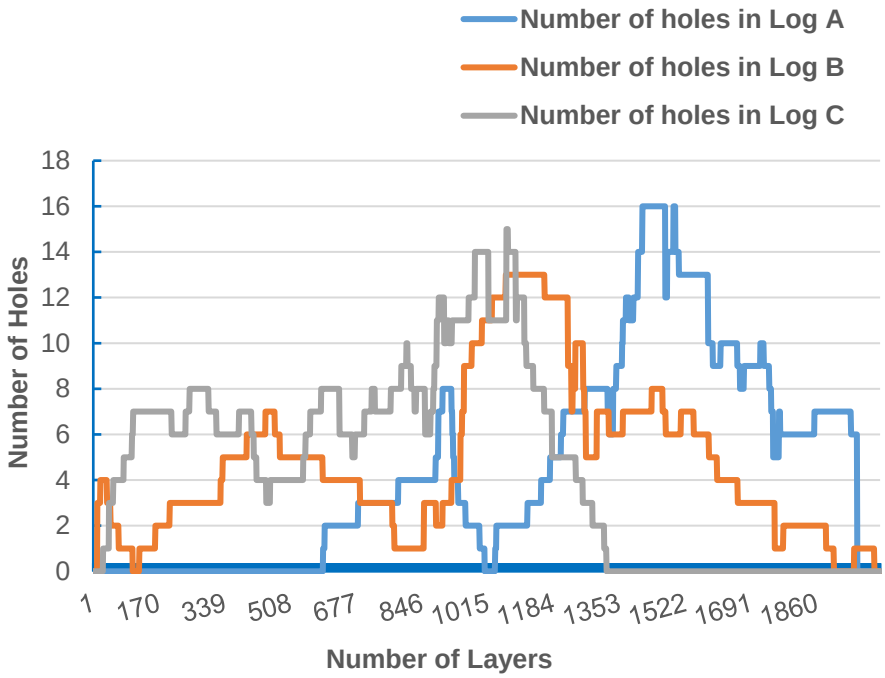

Fig. 3. Statistics on the number of holes in transverse images of three logs

3D Image of Holes

The 3D image of carpenter bee nests was reconstructed based on the projection data collected by CT, as shown in Table 1. There were many holes on the surface of these logs. These holes were the entrance or exit of carpenter bees through the nest, which are marked with red rectangular boxes. At the same position of the reconstructed 3D images, these holes are also marked with red, blue, or green. The carpenter bee nests were distributed inside logs, and therefore it is difficult to obtain the location and shape of these nests from the surface of logs. To show the damage of these logs being eroded by carpenter bees, the reconstructed 3D images were set to 90% transparency by the digital image processing method, and the nests were marked with different colors. It was found that after entering a hole, carpenter bees build nests along the growth direction of logs. Some nests are distributed along the cross-section, and the nests are crisscrossed within the logs. The entrance or exit of a carpenter's nest is represented by orange dots. It can be seen from the directional distribution map of the nests that after entering along with a nest opening, carpenter bees reached the position of the wood's pith core, and then they began to nest along the direction of the growth of the tree's longitudinal axis.

The holes can be clearly seen on the surface of the eave purlin. Carpenter bees usually entered the holes on the surface, and then the cavities extended inward along the log growth direction at the heartwood position, almost avoiding the growth rings formed by early and late wood. These tunnels in the nest had multiple branches that extended along the growth direction of the log. He *et al.* (2017) concluded from the distribution of nests that most nests are parallel branch tunnels or parallel non-branch tunnels. The structural shape of nests were similar to a bamboo joint shape, and up to 10 branch tunnels on the same side could be distributed in parallel. Table 1 extracts the three-dimensional of nests, from which the distribution and shape of the carpenter bee nests can be clearly and intuitively seen, and the tunnels of the nest were mostly distributed in parallel branches.

Table 1. Distribution and Structure of Carpenter Bee Nests

Log Sample	Original Wood	Reconstructed Wood	Nest Perspective	Nest Pore Distribution	Direction of the Nest	
Log A						
Log B						
Log C						

In Table 2, the number, surface area, volume, and log volume of nest connecting domains in Log A, Log B, and Log C were counted, and the volume ratio of nests were also calculated. In this paper, multiple connected nests were counted as a connected domain. There were 5, 8, and 6 carpenter bee nests in Log A, Log B, and Log C, respectively. The minimum and maximum diameters of the nests were 1.04 × 10 mm at Log C1 and 6.56 × 10^2 mm at Log C4. The minimum and maximum surface areas of the nests were 3.26 × 10^2 mm^2 at Log C1 and 2.83 × 10^5 mm^2 at Log C4. The minimum and maximum volumes of the nests were 3.37 × 10^2 mm^3 at Log C1 and 6.06 × 10^5 mm^3 in Log C4. The nest volumes of Log A, Log B, and Log C were 5.05 × 10^5 mm^3, 5.77 × 10^5 mm^3, and 6.11 × 10^5 mm^3, corresponding to 3.1%, 3.4%, and 3.8% of log volume, respectively. These data show that the middle part of the eave purlin was easy to be eroded by carpenter bees, and the volume of nests accounts for 3% to 4% of the total volume. The nest with the smallest diameter was located at the entrance of the carpenter bee nests, and the surface area and volume of these nests reflected damage degree of the carpenter bees to the eave purlin.

The visual analysis of the internal structure of wood components can more visually and intuitively exhibit the internal structure of the distribution of carpenter bee nests. Based on the analysis of the nest volume, the damage degree of carpenter bees to building components can be further known. The nest distribution is related to the service life

(durability) of timber structure buildings, and has greater value for the repair and protection of wood components damaged by carpenter bees.

Table 2. Proportion of Carpenter Bee Nests in Wood

Log Sample	The Number of the Nest	Maximum Nest Width (mm)	Surface Area of Nest (mm^2)	Nest Volume (mm^3)	Total Volume of Nest (mm^3)	Total Volume of Wood (mm^3)	Ratio (%)
Log A	Log A1	1.63E + 02	1.59E + 04	2.92E + 04	5.05E + 05	1.62E + 07	3.12
	Log A2	2.16E + 02	3.63E + 04	7.03E + 04			
	Log A3	4.83E + 02	2.00E + 05	4.05E + 05			
Log B	Log B1	1.79E + 01	9.78E + 02	1.55E + 03	5.77E + 05	1.70E + 07	3.39
	Log B2	2.36E + 01	9.19E + 02	1.37E + 03			
	Log B3	2.38E + 01	1.12E + 03	1.78E + 03			
	Log B4	4.70E + 01	2.53E + 03	4.82E + 03			
	Log B5	6.22E + 01	3.22E + 03	4.82E + 03			
	Log B6	1.93E + 02	1.75E + 04	3.20E + 04			
	Log B7	3.84E + 02	7.98E + 04	1.56E + 05			
	Log B8	4.50E + 02	1.86E + 05	3.74E + 05			
Log C	Log C1	1.04E + 01	3.26E + 02	3.37E + 02	6.11E + 05	1.60E + 07	3.80
	Log C2	1.09E + 01	3.44E + 02	3.81E + 02			
	Log C3	8.13E + 01	3.89E + 03	4.60E + 03			
	Log C4	6.56E + 02	2.83E + 05	6.06E + 05			

Structure of Holes in Three Sections

As shown in Fig. 2, wood is an anisotropic material. Through the comparative observation of transverse sections, radial sections, and tangential sections of wood, the internal structure of wood may be fully understood. In this paper, Log A, Log B, and Log C were scanned to obtain 2D transverse-sectional images. From the transverse sections, radial sections, and tangential sections of each log, 10 section images seriously eroded by carpenter bees were randomly selected. The number and diameter of holes in transverse sections, the number and depth of holes in radial sections, and tangential sections were analyzed. As shown in Table 3, the number of holes in Log B was the largest, with 105 holes.

Table 3. Diameter and Depth of Nests in Three Sections (Num: Number Holes; Max-Dia: Maximum Diameter Width; Min-Dia: Minimum Diameter Width; Max-Dep: Maximum Depth of Nest; Min-Dep: Minimum Depth of Nest)

Sample	Transverse Sections			Radial Sections			Tangential Sections		
	Num	Max-Dia (mm)	Min-Dia (mm)	Num	Max-Dep (mm)	Min-Dep (mm)	Num	Max-Dept (mm)	Min-Dep (mm)
Log A	88	1.64E + 01	9.45E + 00	536	2.80E + 02	1.24E + 01	251	1.40E + 02	1.23E + 01
Log B	105	1.83E + 01	8.75E + 00	628	3.59E + 02	2.24E + 01	278	1.56E + 02	1.76E + 01
Log C	78	1.98E + 01	1.05E + 01	540	2.35E + 02	1.25E + 01	312	2.76E + 02	1.92E + 01

There were only 78 holes in Log C, but the average diameter of these holes was the largest. In these radial sections, the maximum number of holes in Log B was 628, and the maximum depth of these holes was 358.6 mm. In these tangential sections, the maximum number of holes in Log C was 312 and the depth was the maximum. Among the three logs, the number and maximum depth of holes on the tangential sections were less than those on the radial sections. Therefore, it can be seen that carpenter bees were more likely to erode the wood close to the pith of logs.

Carpenter bee nests are randomly generated in 3D space, which cannot be observed and analyzed from a certain perspective. These nests can be accurately located and displayed on each section. According to the analysis, these radial sections of the eave purlin were the most seriously eroded by carpenter bees, and the size and number of holes were the largest. The conclusion is consistent with the results of Eriksen *et al*. (2016) regarding the harm of worms to the three sections of wood.

Mechanical Property Analysis

If one end of the log A is fixed, and then 10000 N of directional force is applied parallel to the axial direction of the log at the other end. According to the parameters set in the 3D images reconstruction section of the experimental part, the directional force results in Table 4 can were obtained. Log B and log C also operated in the same way. Table 4 shows the position of the first hot spot of the maximum stress of Log A, Log B, and Log C in the x, y, and z coordinate system after the directional force was applied. The mean value stresses of Log A, Log B, and Log C were 6.16×10^5 Pa, 1.28×10^6 Pa, and 8.95×10^5 Pa, respectively. The volume at the hot spot with the maximum stress was 3.78×10^3 mm³, 1.01×10^2 mm³, and 7.09×10^2 mm³, respectively. The mean value stress at the maximum hot spot of Log B was the largest, but the volume of stress failure was the smallest.

Table 4. Directional Force and Torque at the Maximum Hot Spot

Mechanics	Sample	Max. Value (Pa)	Min. Value (Pa)	Mean Value (Pa)	Std. Deviation (Pa)	Volume (mm³)	Max. Value x (mm)	Max. Value y (mm)	Max. Value z (mm)
Directional Force	Log A	1.25E + 06	5.51E + 05	6.16E + 05	9.61E + 04	3.78E + 03	-9.02E + 00	-4.82E + 01	-2.29E + 02
	Log B	2.09E + 06	9.33E + 05	1.28E + 06	3.45E + 05	1.01E + 02	3.31E + 00	-3.06E + 02	1.36E + 00
	Log C	1.45E + 06	5.63E + 05	8.95E + 05	2.51E + 05	7.09E + 02	-1.45E + 01	4.22E + 01	2.17E + 02
Torque	Log A	1.10E + 07	2.89E + 06	3.97E + 06	1.18E + 06	1.77E + 04	-3.70E + 01	-2.03E + 01	-2.34E + 02
	Log B	1.08E + 07	9.41E + 06	1.01E + 07	7.01E + 05	2.53E + 01	-2.81E + 01	-4.85E + 01	-1.82E + 02
	Log C	1.17E + 07	3.38E + 06	4.71E + 06	1.47E + 06	8.11E + 03	4.49E + 01	2.24E + 01	-5.33E + 02

One end of the log A was fixed, and 1000 N torque was applied to the other end. According to the parameters set in the section 3D images reconstruction of the experimental part, the torque results in Table 4 were obtained. Log B and log C operated in the same way. Table 4 shows the position of the first hot spot of the maximum stress of Log A, Log B, and Log C in the x, y, and z coordinate system after torque was applied. The mean value stresses of Log A, Log B, and Log C were 3.97×10^6 Pa, 1.01×10^7 Pa, and 4.71×10^6 Pa, respectively. The volume at the hot spot with the maximum stress was 1.77×10^4 Pa, 2.53×10 mm³, and 8.11×10^3 mm³, respectively. This was related to the volume distribution of carpenter bees on the three sections of logs. The number of Log B nest connected domains was 8, the distribution was relatively scattered, and the volume of damage in the stress range was small. The number of connected domains of Log A and Log C nests was 3 or 4, respectively. The distribution of the nests was relatively concentrated, and the volume damaged by stress was large.

Figures 4 and 5 show the hot spot distribution of the eaves purlin after being subjected to the maximum stress. The position of the maximum stress hot spots in the top view (a), front view (b) and right view (c) are marked with red crosses and circles. In the stereogram (d), the positions of the fixed end and the stressed end of the log can be clearly seen, which are represented by red and green respectively. The directional force is represented by the vertical arrow and the torque is represented by the rotation arrow.

From Fig. 4, Log A, Log B, and Log C, it is possible to see the location and range of the maximum hot spot distribution of the maximum stress after directional force is applied. In the top view (a) of Log A and Log C, the position of the hot spot with the maximum stress occurred at the edge hole, and in the top view (a) of Log B, the position of the hot spot with the maximum stress was located at the larger part of the internal hole. It can be seen from the front view (b) and right view (c) of Log A, Log B and Log C that the hot spots with the maximum stress were mostly in the places with dense concentrations of holes. It is concluded that holes will reduce the mechanical properties of wood, and the directional force has a great influence on holes.

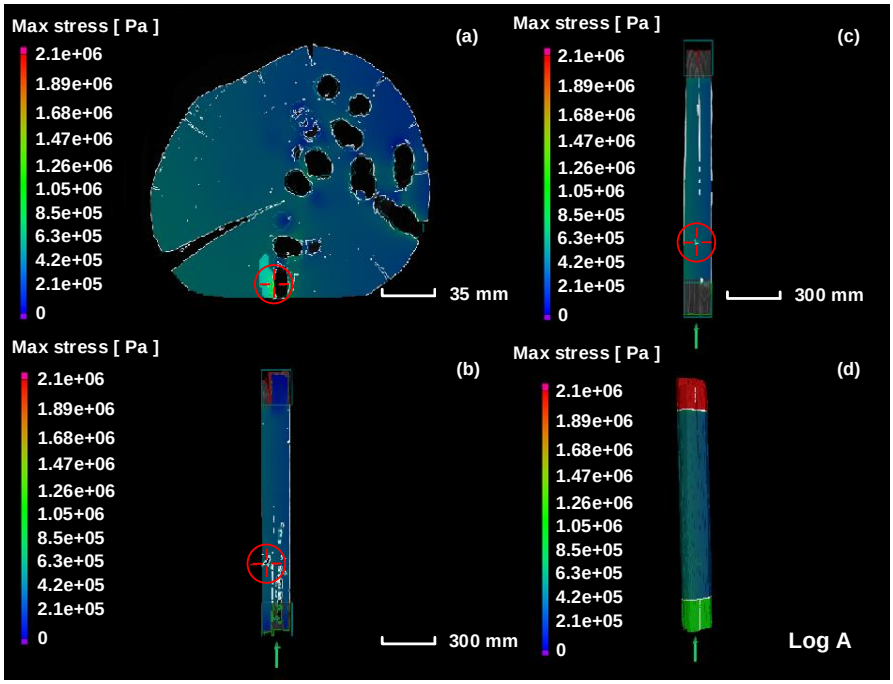

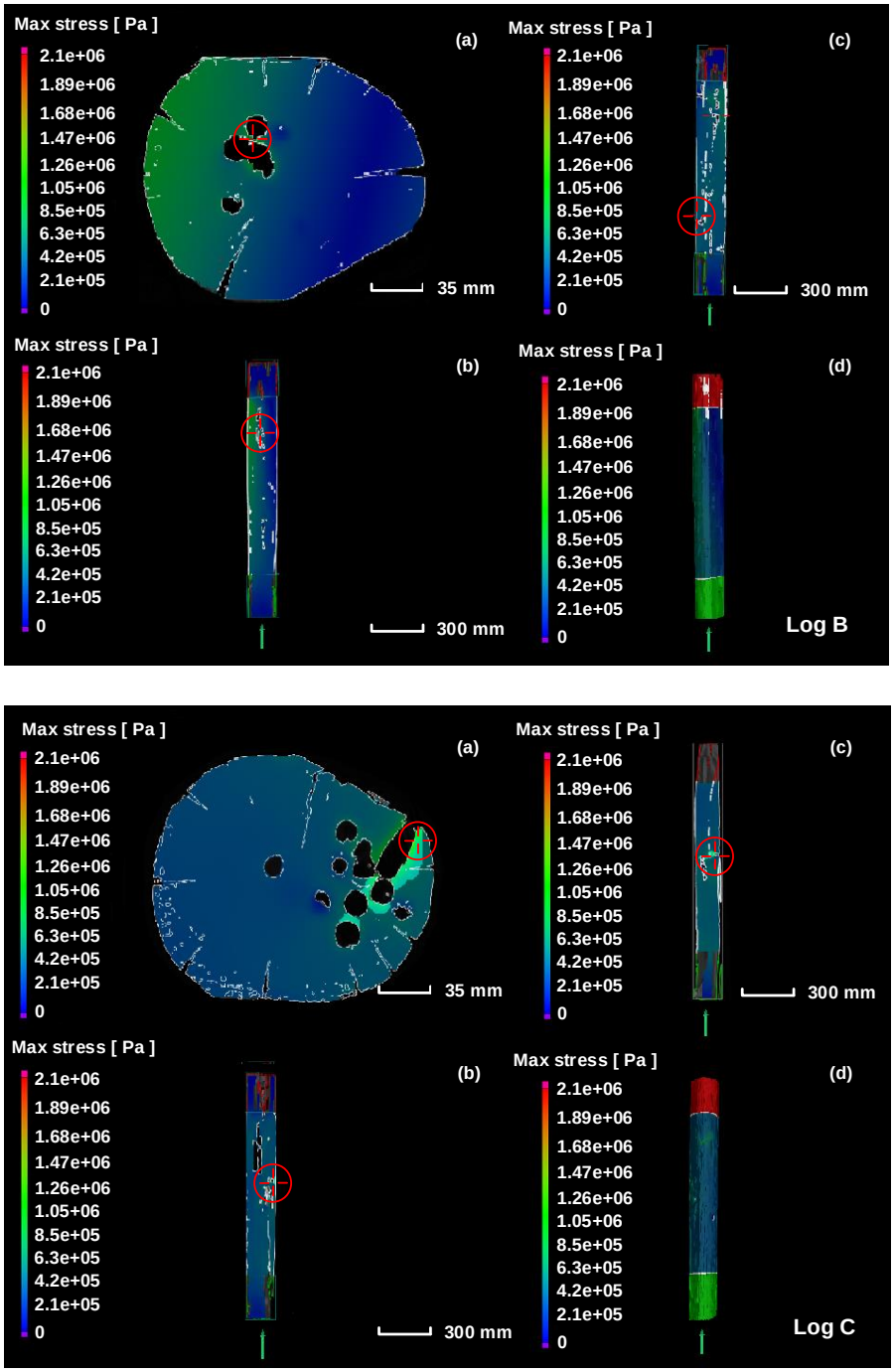

Fig. 4. Figure 4 shows the simulation results of three logs (Log A, Log B, Log C) under the directional force; (a) Represents a top view; (b) represents a front view; (c) Represents the right view; (d) Represents a stereogram

From Fig. 5, Log A, Log B, and Log C, one can see the location and range of the maximum hot spot distribution of the maximum stress after the torque force is applied. In the top view (a) of Log A, Log B and Log C, the hot spot with the maximum stress was located at the large crack.

According to the front view (b) and right view (c) of Log A, Log B and Log C, the hot spot of the maximum stress also occurred at the edge crack or large crack. It is concluded that cracks will reduce the mechanical properties of wood, and the torsion has a great influence on cracks.

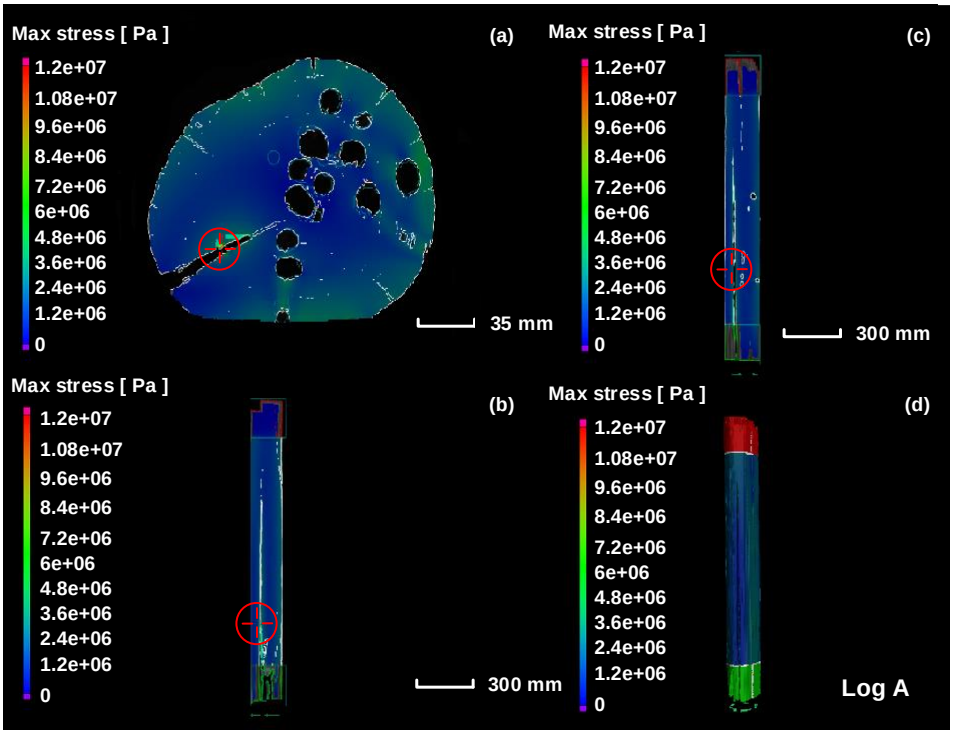

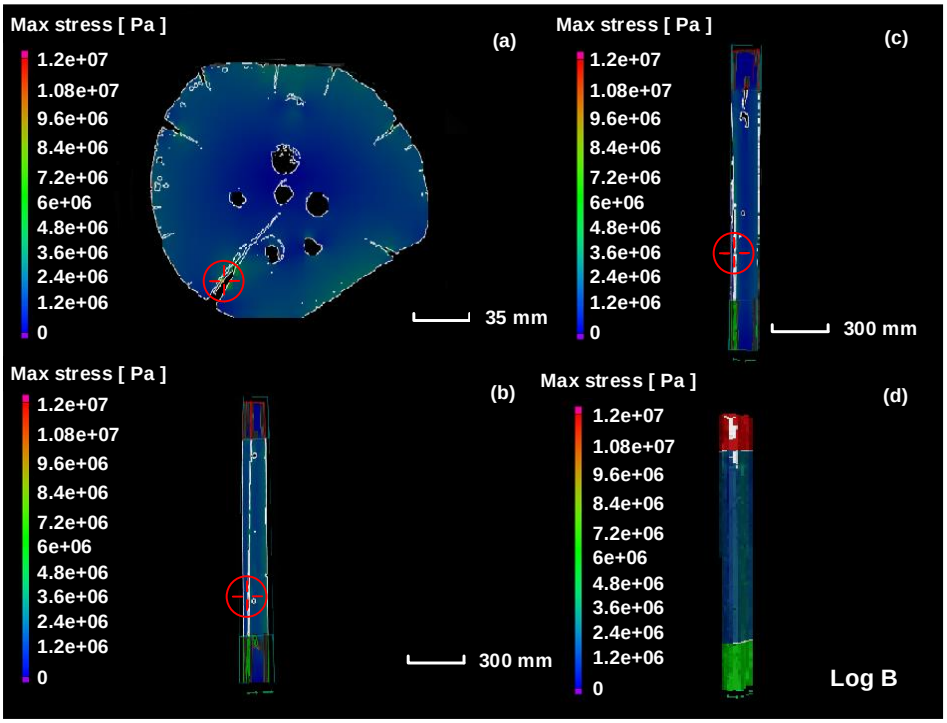

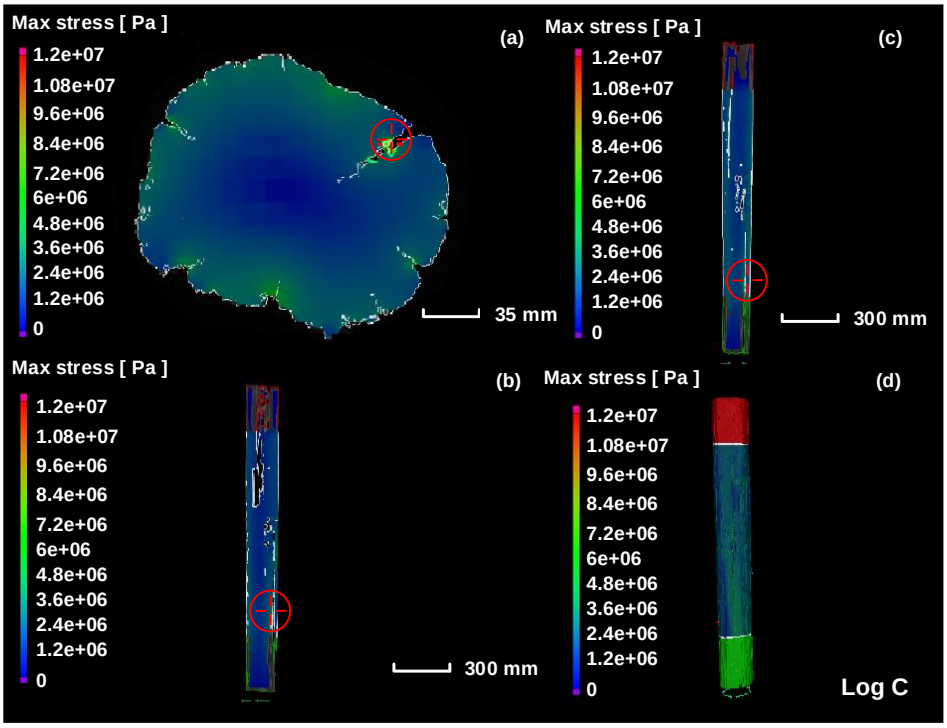

Fig. 5. Figure 5 shows the simulation results of three logs (Log A, Log B, Log C) under the torque force; (a) Represents a top view; (b) represents a front view; (c) Represents the right view;(d) Represents a stereogram

CONCLUSIONS

1. Computed tomography has been widely used in the research of wood, but it is less used in the simulation analysis of the distribution law and mechanical properties of carpenter bee nests in timber building components. In this paper, the internal structure of components damaged by carpenter bees was visualized and analyzed, which not only made the carpenter bee nests clear and intuitive, but also showed that the radial sections were most damaged by carpenter bees, and the nest volume accounted for 3% to 4% of the eave purlin.
2. It was a random behavior by which timber buildings were eroded by carpenter bees. Each research object showed different situations, but the distribution of carpenter bee nests and the harm to such components had similar results. Carpenter bee nests were distributed along the axial direction of the eaves purlin and widely in the radial sections. The material density within latewood is high, so carpenter bees avoided the growth rings of trees when building nests.
3. The mechanical simulation analysis of the components damaged by carpenter bees showed that after the directional force was applied, the hot spot of the maximum stress occurred at the hole. After torsion was applied, the hot spot of the maximum stress occurred at the larger crack.
4. Carpenter bee nests have an impact on wood, and cracks further reduce the mechanical properties of timber building components. For the detection of timber building components, the holes and cracks generated due to the change of moisture content in

timber buildings should be of concern, and then the timber buildings should be protected and repaired.

ACKNOWLEDGEMENTS

This study was funded by the Natural Science Foundation of Shandong Province, China (Grant No. ZR2020QC174), the Application of Computed Tomography (CT) Scanning Technology to Damage Detection of Timber Frames of Architectural Heritage, and the Taishan Scholar Project of Shandong Province, China (Grant No. 2015162).

REFERENCES CITED

Annila, P. J., Lahdensivu, J., Suonketo, J., Pentti, M., and Vinha, J. (2018). "Need to repair moisture-and mould damage in different structures in Finnish public buildings," *Journal of Building Engineering* 16, 72-78. DOI: 10.1016/j.jobe.2017.12.010

Azmi, W. A., Ghazi, R., and Mojamed, N. Z. (2012). "The importance of carpenter bees, *Xylocopa varipuncta* (Hymenoptera: Apidae) as pollination agent for mangrove community of Setiu Wetlands, Terengganu, Malaysia," *Sains Malaysiana* 41(9), 1057-1062.

Bukauskas, A., Mayencourt, P., Shepherd, P., Sharma, B., Mueller, C., Walker, P., and Bregulla, J. (2019). "Whole timber construction: A state of the art review," *Construction and Building Materials* 213, 748-769. DOI: 10.1016/j.conbuildmat.2019.03.043

Charles, F., Coston-Guarini, J., Guarini, J., and Lantoine, F. (2018). "It's what's inside that counts: Computer-aided tomography for evaluating the rate and extent of wood consumption by shipworms," *Journal of Wood Science* 64(4), 427-435. DOI: 10.1007/s10086-018-1716-x

Du, X., Feng, H., Hu, M., Fang, Y., and Chen, S. (2018). "Three-dimensional stress wave imaging of wood internal defects using TKriging method," *Computers and Electronics in Agriculture* 148, 63-71. DOI: 10.1016/j.compag.2018.03.005

Eriksen, A. M., Gregory, D. J., Villa, C., Lynnerup, N., Botfeldt, K. B., and Rasmussen, A. R. (2016). "The effects of wood anisotropy on the mode of attack by the woodborer *Teredo navalis* and the implications for underwater cultural heritage," *International Biodeterioration & Biodegradation* 107, 117-122. DOI: 10.1016/j.ibiod.2015.11.018

Ge, Z., Chen, L., Luo, R., Wang, Y., and Zhou, Y. (2018). "The detection of structure in wood by X-ray CT imaging technique," *BioResources* 13(2), 3674-3685. DOI: 10.15376/biores.13.2.3674-3685

He, C., Zhu, C., and Wu, Y. (2017). "Morphology and nesting behavior of *Xylocopa rufipes* (Hymenoptera: Apidae)," *Acta Entomologica Sinica* 60(9), 1074-1082.

Jiao, J., Xia, Q., and Shi, F. (2019). "Nondestructive inspection of a brick-timber structure in a modern architectural heritage building: Lecture hall of the Anyuan Miners' Club, China," *Frontiers of Architectural Research* 8(3), 348-358. DOI: 10.1016/j.foar.2019.06.005

Llana, D. F., Short, I., and Harte, A. M. (2020). "Use of non-destructive test methods on Irish hardwood standing trees and small-diameter round timber for prediction of mechanical properties," *Annals of Forest Science* 77(3), Article Number 62. DOI: 10.1007/s13595-020-00957-x

Ma, X. X., Wang, L., Zhu, H. Y., Liu, B., Zhang, B., Lu. Y., Wang, Y. H., Jian, M. L., and Wang, L. R. (2019). "Risk zones of carpenter bees for wooden structure of ancient building in China," *Scientia Silvae Sinicae* 57(4), 116-123. DOI: 10.11707/ j.1001-7488.20210412

Pan, L., Rogulin, R., and Kondrashev, S. (2021). "Artificial neural network for defect detection in CT images of wood," *Computers and Electronics in Agriculture* 187(C), article ID 106312. DOI: 10.1016/j.compag.2021.106312

Pando, J. B., Tchuenguem, F., and Tamesse, J. L. (2011). "Foraging and pollination behaviour of *Xylocopacalens Lepeletier* (Hymenoptera: Apidae) on *Phaseolus coccineus* L. (Fabaceae) flowers at Yaounde (Cameroon)," *Entomological Research* 41(5), 185-193. DOI: 10.1111/j.1748-5967.2011. 00334.x

Rashidi, M., Hoshyar, A. N., Smith, L., Bijan, S., and Siddique, R. (2020). "A comprehensive taxonomy for structure and material deficiencies, preventions and remedies of timber bridges," *Journal of Building Engineering* 34(9), article ID 101624. DOI: 10.1016/j.jobe.2020.101624

Sousa, H. S., Branco, J. M., and Lourenço, P. B. (2013). "Effectiveness and subjectivity of visual inspection as a method to assess bending stiffness and strength of chestnut elements," *Advanced Materials Research* 778, 175-182. DOI: 10.4028/www.scientific.net/AMR.778.175

Vössing, K. J., and Niederleithinger, E. (2018). "Nondestructive assessment and imaging methods for internal inspection of timber. A review," *Holzforschung* 172(6), 467-476. DOI: 10.1515/hf-2017-0122

Wei, Q., Leblon, B., and La Rocque, A. (2011). "On the use of X-ray computed tomography for determining wood properties: A review," *Canadian Journal of Forest Research* 41(11), 2120-2140. DOI: 10.1139/x11-111

You, Z. S. (2016). "Study on Wu's mansion in Fengqi, Zherong County," *Fujian Cultural and Expo Journals* 2016(1), 61-65.

Zhang, D., Yu, Y., Guan, C., Wang, H., Zhang, H., and Xin, Z. (2021). "Nondestructive testing of defect condition of wall wood columns in Yangxin Hall of the Palace Museum, Beijing," *Journal of Beijing Forestry University* 43(5), 127-139.

Article submitted: January 6, 2022; Peer review completed: February 26, 2022; Revised version received and accepted: March 3, 2022; Published: March 7, 2022.
DOI: 10.15376/biores.17.2.2443-2456